

An inverse approach to estimate bubble-mediated air-sea gas flux from inert gas measurements

David P. Nicholson¹, Steven R. Emerson², Samar Khatiwala³
and Roberta C. Hamme⁴

¹ *Marine Chemistry and Geochemistry Department, Woods Hole Oceanographic Institution, 266 Woods Hole Road, Woods Hole, MA 02543, USA, E-mail: dnicholson@whoi.edu*

² *School of Oceanography, University of Washington, PO Box 357940, Seattle, WA, USA, E-mail: emerson@u.washington.edu*

³ *Lamont Doherty Earth Observatory of Columbia University, PO Box 357940, Palisades, NY, USA, E-mail: spk@ldeo.columbia.edu*

⁴ *School of Earth and Ocean Sciences, University of Victoria, Victoria, BC V8W 3V6, Canada, E-mail: rhamme@uvic.ca*

Abstract. An ocean general circulation model (oGCM) was used in concert with a global database of inert gas measurements (Ne, Ar, N₂/Ar and Kr/Ar) to constrain the magnitude of bubble mediated air-sea gas flux. We illustrate the inverse method using a simple bubble model that includes two end member types of bubbles: small bubbles that completely dissolve, and larger bubbles that briefly are submerged and exchange gases with seawater. An inverse solution to the oGCM constrains the flux contribution for bubbles that completely dissolve as a function of wind speed. Our results indicate air injection values at high wind speeds ($> 10 \text{ m s}^{-1}$) that fall between two previous estimates which differ by a factor of three. Future improvements of the method demonstrated here but including seasonality should allow for better constraints on bubble mediated gas exchange as well as the ability to test the performance of a range of bubble models.

Key Words: bubble fluxes, noble gases, air-sea exchange

1. Introduction

The flux of gases across the air-sea interface commonly is parameterized as the product of a gas transfer coefficient, k , and the air-sea concentration gradient of a gas such that,

$$F_{as} = -k_c([C] - \alpha_c p_c) \quad \text{or} \quad F_{as} = -k_c([C] - [C]_{eq}^{slp}) \quad (1)$$

where $[C]$ (mol m^{-3}) is the dissolved concentration of gas C , α_c ($\text{mol m}^{-3} \text{ atm}^{-1}$) is the solubility of the gas, p_c (atm) is the partial pressure of the gas in the overlying

atmosphere, and $[C]_{eq}^{slp}$ is the dissolved concentration in equilibrium with local sea level pressure (*slp*). As convention here, a positive flux is from atmosphere to ocean. Such a description of air-sea exchange only accounts for surface diffusive exchange and does not accommodate the role of bubbles. For example, for a steady-state mixed layer where $F_{as}=0$, Equation 1 requires the mixed layer to be in equilibrium with the atmosphere (i.e. $[C]=[C]_{eq}^{slp}$). Observations of insoluble gases, however, have revealed persistent supersaturation of gases such as He, Ne and Ar (Craig and Hayward 1987; Craig and Weiss 1971; Spitzer and Jenkins 1989). The observed steady-state supersaturation is due to bubble processes, which cause an asymmetry between the diffusive transfer rate of gases into and out of the surface ocean (Keeling 1993). A more complete description of air-sea gas exchange should thus include an additional description of bubbles that cannot be encompassed in the transfer velocity term. We can then modify Equation 1 as such:

$$F_{as} = -k_c([C] - [C]_{eq}^{slp}) + F_{bub} \quad (2)$$

where F_{bub} is the air-sea bubble flux. Including a bubble term has several important consequences for air-sea gas exchange: 1. Total air-sea flux is not strictly proportional to the air-sea concentration gradient; 2. Steady-state gas concentration is greater than atmospheric equilibrium; and 3. While the relative diffusive fluxes of gases can be proportionally related by the Schmidt number to the 0.5 power, bubble fluxes can have very different scaling, depending also on gas solubility and diffusivity (Keeling 1993).

The saturation anomaly of inert gases, including Ne, N₂, Ar and Kr, record valuable information about the physical processes that exchange gases between the atmosphere and ocean. In particular, they are powerful tracers of the influence of bubble mediated processes in air-sea gas exchange. Studies of these gases have been applied to constrain the air-sea bubble flux at specific study sites, by combining 1-D modeling with a time-series of inert gas observations (Hamme and Emerson 2006; Hamme and Severinghaus 2007; Stanley *et al.* 2009). In this paper, we extend previous work to the global scale, by combining a database of inert gas observations with an ocean general circulation model (oGCM) to evaluate the magnitude and spatial distribution of bubble mediated air-sea gas flux. Through an inverse modeling approach, we constrain the magnitude of gas flux based on a simple wind speed dependent bubble model that includes both small collapsing bubbles and large exchanging bubbles.

2. Background

2.1 Inert gas properties

The interior distributions of inert gases Ne, N₂, Ar and Kr are useful as tracers of air-sea interactions because these gases have no significant sources or sinks in the ocean interior. The observed gas concentration in the interior can thus be considered to be due only to air-sea processes during outcrop and transport since subduction. Each of these gases is well mixed in the atmosphere, resulting in a known boundary condition. To a first order approximation, these gases dissolve in seawater in equilibrium with the atmosphere, according to Henry's Law which states that dissolved concentration is the product of gas solubility and partial pressure of the gas in air. Gas solubility in seawater is a function of temperature and salinity. Small observed deviations from equilibrium make these gases useful as tracers. We therefore report seawater dissolved gas concentration as a saturation anomaly, which is the percentage deviation from equilibrium with the atmosphere at a reference pressure of 1 atm using a delta notation:

$$\Delta C = \frac{[C] - [C]_{eq}^{ref}}{[C]_{eq}^{ref}} \text{ or for a ratio of gases, } \Delta C_1/C_2 = \frac{C_1/C_2 - (C_1/C_2)_{eq}}{(C_1/C_2)_{eq}} \quad (3)$$

where $[C]_{eq}^{ref}$ is equilibrium at 1 atm and C_1/C_2 is the ratio of two gases. Equilibrium solubilities were calculated from previous laboratory measurements (Hamme and Emerson 2004; Weiss and Kyser 1978).

Analytically, we have measured the saturation anomaly of some gases directly by isotope dilution (Ne and Ar), while others are measured only in ratio to Ar and thus are reported as gas ratios (Kr/Ar and N₂/Ar). A gas ratio can be more precisely measured analytically on a mass spectrometer than can an absolute gas concentration (Hamme and Severinghaus 2007; Nicholson *et al.* 2010). An additional advantage of using gas ratios is that atmospheric pressure variations affect each gas equally, cancelling when considering the ratio of two gases and thus do not impact the gas ratio saturation anomaly.

Multiple gas tracers are used to isolate the physical processes that cause dissolved gases to deviate from equilibrium (Figure 1). The saturation anomaly of an inert gas is influenced by cooling/warming, atmospheric pressure variations, and mixing, as well as bubble processes, requiring multiple gas tracers to isolate the bubble effect. Cooling causes undersaturation due to the temperature dependent solubility of gases. Mixing causes supersaturation because of the non-linearity of the solubility function of gases (Ito and Deutsch 2006) and is most important in the thermocline where mixing occurs across strong temperature gradients.

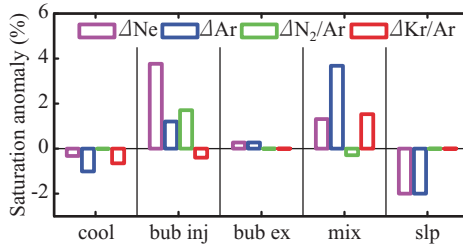


Figure 1 The sensitivity of each gas tracer to cooling (-100 W m^{-2}), bubble injection ($u_{10} = 10 \text{ m s}^{-1}$), bubble exchange ($u_{10} = 10 \text{ m s}^{-1}$), mixing (equal parts 5°C and 25°C water) and sea level pressure (2% below 1 atm).

Atmospheric pressure variations cause the true equilibrium concentration to deviate from equilibrium referenced to standard pressure (1 atm).

2.2 Parameterizing bubble fluxes

A full theoretical description of bubble mediated gas flux depends on several properties of the bubble dynamics that are difficult to quantify, such as bubble penetration depth, size spectrum, population, rise velocity, etc (Keeling 1993). A promising approach to parameterizing bubble flux (F_{bub} ; $\text{mol m}^{-2} \text{ s}^{-1}$) has been to represent the flux due to the spectrum of bubble sizes as the sum of the contributions of two end-member bubble types: (i) small bubbles that completely collapse, injecting their entire contents (V_{inj}), and (ii) large bubbles that exchange diffusively while briefly submerged, before rising back to the surface (V_{ex}) (Fuchs *et al.* 1987; Jenkins *et al.* 1988; Keeling 1993; Spitzer and Jenkins 1989; Stanley *et al.* 2009). The first process depends only on the injection rate and the atmospheric partial pressure of the gas, p_c (atm), while the exchange process also depends on solubility, α_c and molecular diffusivity (D_c ; $\text{m}^2 \text{ s}^{-1}$) of the specific gas such that

$$F_{\text{bub}} = \left(V_{\text{inj}} + V_{\text{ex}} \left(\frac{D_c}{D_0} \right)^x \left(\frac{\alpha_c}{\alpha_0} \right)^y \right) p_c \quad (4)$$

where the exponents x and y are set to 0.5 and 1, respectively (Hamme and Emerson 2006; Keeling 1993). D_0 and α_0 are unit-normalization constants with values of $1 \text{ m}^2 \text{ s}^{-1}$ and $1 \text{ mol m}^{-3} \text{ atm}^{-1}$, respectively.

Additionally, the flux of injecting and exchanging bubbles was considered to scale proportionally to whitecap coverage, which has been demonstrated to scale as a function of $(u_{10} - 2.27)^3$ where u_{10} is 10-meter wind speed (m s^{-1}) ($F_{\text{bub}} = 0$ for $u_{10} < 2.27$) (Monahan and Torgersen 1990). Combining the whitecap dependence with Equations 2 and 4 gives an expression for total air-sea flux of

$$F_{as} = -k_c([C] - [C]_{eq}^{slp}) + A_{inj}P_c(u_{10} - 2.27)^3 + A_{ex}P_c\left(\frac{D_c}{D_0}\right)^{0.5}\left(\frac{\alpha_c}{\alpha_0}\right)(u_{10} - 2.27)^3 \quad (5)$$

where A_{inj} and A_{ex} are spatially invariant constants that determine the magnitude of injecting and exchanging bubbles. The goal of this paper is to use inert gas observations to constrain the terms A_{inj} and A_{ex} that control the magnitude of bubble flux as a function of wind speed. In the future, the modeling methodology described herein can also be applied to more advanced and varied descriptions of bubble mediated gas exchange than described in (5).

3. Methods

3.1 Data

To constrain bubble fluxes, we use previously published observations of dissolved Ne, Ar, N₂/Ar and Kr/Ar ratios. Neon observations were included from profiles collected from 1998-2001 at the Bermuda Atlantic Time-series Study (BATS, 30°40' N, 64°10' W), the Hawaii Ocean Time-series (HOT, 22°45'N, 158°W) and the Kyodo North Pacific Ocean Time-series (KNOT, 44°N, 155°E) (Hamme and Emerson 2002). We include Ar and N₂/Ar measurements from HOT, BATS [Hamme, 2003] and a Northwest Pacific site (NWP, 47°N 167°E) (Nicholson *et al.* 2010). Kr/Ar was measured on profiles of samples from NWP, a site in the subtropical North Pacific (STNP, 26°N 152°W) and a site in the eastern tropical Atlantic (ETA, 10°N 27°W) (Nicholson *et al.* 2010). In total, 699 measurements are included, 244 of Ar, 186 of Ne, 243 of N₂/Ar and 26 of Kr/Ar.

3.2 Model

The transport matrix method for simulating tracers (Khatiwala 2007; Khatiwala *et al.* 2005) is based on the concept that the advection-diffusion transport of a GCM can be encoded into a sparse matrix of linear equations. The resulting matrix can then be used to directly calculate the steady-state distribution of a tracer. Steady-state transport of a passive tracer in a GCM can be described as

$$\frac{d\mathbf{c}}{dt} = 0 = \overline{\mathbf{A}}\mathbf{c} + \mathbf{q} \quad (6)$$

where \mathbf{c} is a vector of tracer concentrations of length N , where N is the total number of grid boxes in the GCM. $\overline{\mathbf{A}}$ is a matrix of N by N size, which represents the annual mean transport of tracer due to advection, diffusion and parameterized sub-grid scale model processes that occurs within a timestep of dt . \mathbf{q} is a vector of length N that represents any sources or sinks of the tracer at each grid point.

For the inert gases of interest, the only source/sink term contributing to \mathbf{q} is at the air-sea surface boxes. \mathbf{q} for all interior boxes is equal to zero. Solving Equation 6 for \mathbf{c} gives the steady-state model solution. When $\bar{\mathbf{A}}$ is known, steady-state solution can be reached by inverting the sparse matrix $\bar{\mathbf{A}}$ instead of requiring a time consuming integration.

The steady-state solution depends on the formulation of the transport matrix $\bar{\mathbf{A}}$. This matrix is created not from any explicit solution, but instead from empirically probing a GCM with a passive tracer. For this work, we use a transport matrix, $\bar{\mathbf{A}}$, created from the 2.8° resolution seasonally forced version of the MIT ocean GCM (MITgcm) (Khaliwala *et al.* 2005; Marshall *et al.* 1997). The MITgcm model has 15 vertical levels and is forced with monthly mean climatology (Jiang *et al.* 1999; Trenberth *et al.* 1989) and surface temperature and salinity are weakly restored to Levitus climatology. Compared to observations, this model tends to be more rapidly ventilated in the North Pacific and subpolar North Atlantic and to exhibit somewhat sluggish ventilation of Antarctic bottom waters (Dutay *et al.* 2002; Matsumoto *et al.* 2004).

The transport matrix $\bar{\mathbf{A}}$ is based on annual mean circulation, and thus annual mean heat transport and air-sea flux. Since cooling driven gas anomalies depend on the balance of heat flux and wind speed, annual mean winds are the most appropriate choice of wind product to be used with annual mean circulation. For air-sea gas flux calculations, slp and u_{10} are based on NCEP reanalysis long term mean climatology (Kistler *et al.* 2001). Gas transfer, k_c , is calculated from u_{10} using a quadratic wind speed relationship (Sweeney *et al.* 2007). F_{as} (both for diffusive and bubble fluxes) is scaled by $(1-f_{ice})$ where f_{ice} is fractional winter ice cover from ocmip-2 (Zwally *et al.* 1983).

4. Results

4.1 Inverse solution

In section 3.1 we described how gas saturation anomaly depends on cooling, atmospheric pressure, mixing, injecting bubbles and exchanging bubbles. Using field observations we can constrain the role of each using an inverse approach. Because each process only causes a small deviation from equilibrium, observed gas disequilibrium (ΔC_{obs}) is well approximated as the sum of the disequilibrium of each effect so that

$$\Delta C_{obs} = \Delta C_{slp} + \Delta C_{mix} + \Delta C_{cool} + \Delta C_{inj} + \Delta C_{ex} \quad (7)$$

where the subscripts slp , mix , $circ$, inj and ex refer to saturation anomaly due to pressure variations, interior mixing, diffusive surface exchange and circulation,

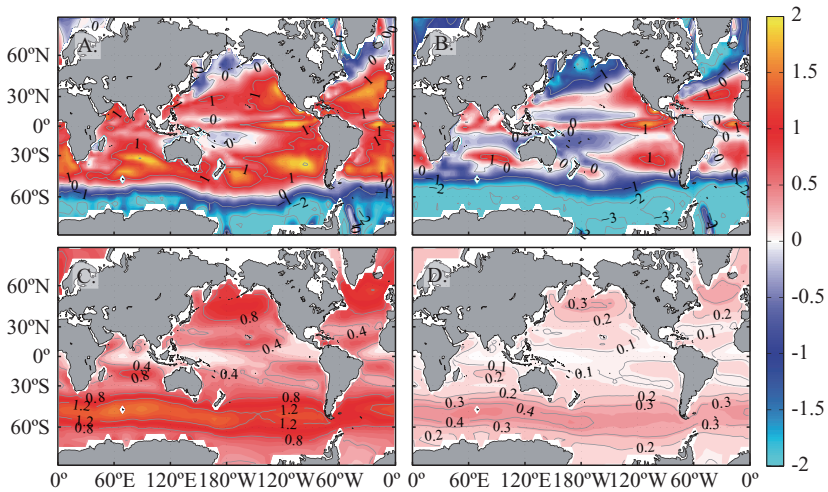


Figure 2 Surface ΔAr due to (A) All processes, (B) Cooling, circulation and pressure (C) Bubble injection and (D) Bubble exchange. Lighter gases will have larger magnitude for (C) and smaller magnitude for (B) relative to Ar, and vice-versa for heavier gases.

bubble injection and bubble exchange, respectively.

A series of seasonally steady-state model solutions were computed to isolate each physical process (Figure 2). First (*run1*) was computed with no bubble flux, such that air-sea flux is calculated using Equation 1 with no bubble flux. Thus, *run1* encompasses the effects of *slp*, *mix* and *circ*. For *run1*, low atmospheric pressure and cooling causes a negative saturation anomaly at high latitudes and western boundary currents while positive anomalies are largest in upwelling water that is warming (Figure 2B). Next, two runs were completed with the air-sea flux as described in Equation 4 but one run had only injecting bubble flux (*run2*) and the other had only exchanging bubble flux (*run3*). The effect of bubble fluxes is the difference between these runs and *run1*, which had no bubble flux. Supersaturation due to injection flux (*run2*-*run1*) and exchanging flux (*run3*-*run1*) where largest in windy areas (Figure 2C and 2D), and injection bubble flux was overall larger than the exchange flux. For *run2* and *run3*, A_{inj} and A_{ex} were each set to an initial guess value of the correct order of magnitude. The final constrained values of A_{inj} and A_{ex} did not depend on the initial guess. To isolate the bubble components, Equation 7 can then be rewritten as:

$$\Delta C_{obs} - \Delta C_{run1} = A_{inj}(\Delta C_{run2} - \Delta C_{run1}) + A_{ex}(\Delta C_{run3} - \Delta C_{run1}) \quad (8)$$

A linear equation of the form shown above can be written for each of the 699 observations by linearly interpolating the results of each run to the location of each observation. In matrix notation this can be represented as an overdetermined

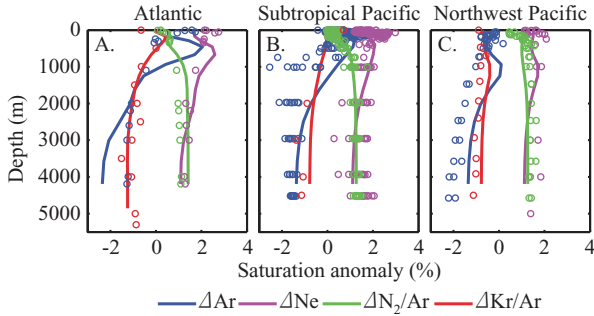


Figure 3 Observations (circles) compared to model results for (A) the Atlantic (BATS and ETA) (B) the Subtropical Pacific (HOT and STNP) and (C) the Northwest Pacific (NWP).

system of 699 equations and two unknowns:

$$\mathbf{c} = \mathbf{B}\mathbf{x} \quad (9)$$

where \mathbf{c} is the column vector containing the left hand of Equation 8, \mathbf{B} contains the model run terms on the right side, and \mathbf{x} is the column vector $[A_{inj}; A_{ex}]$. The least squares solution for \mathbf{x} yielded values and standard error of $A_{inj} = 2.51 \times 10^{-9} \pm 0.19 \times 10^{-9}$ (7.4%) ($\text{mol s}^2 \text{m}^{-5} \text{atm}^{-1}$) and $A_{ex} = 1.15 \times 10^{-5} \pm 0.80 \times 10^{-6}$ (69.2%) ($\text{mol s}^2 \text{m}^{-5} \text{atm}^{-1}$). Error estimates were calculated by multiplying the standard error of the least squares inversion calculation multiplied by the Student's t-test value for two standard deviations and 12 degrees of freedom. The number of degrees of freedom in inert gas distributions should be significantly less than the number of observations. As a rough estimate, we assigned one degree of freedom to each gas or gas ratio, for each profile location, resulting in 12 degrees of freedom (4 types of measurements \times 3 locations for each). The error estimates do not take into account errors from difficult to quantify uncertainties in the gas transfer coefficient (k), NCEP forcing products, or in model circulation.

While model results generally compare well with observations (Figure 3), there are several important implications of using annual mean circulation and wind forcing for our model inversion, due to the inability to resolve seasonality. In the upper ocean, gas saturation state varies seasonally, thus comparing individual observations to the model adds scatter. For the ocean interior, gas signatures originally subducted at high latitudes may be primarily influenced by winter conditions rather than the annual mean. For example, from the gas tracers more sensitive to cooling ($\Delta\text{Kr}/\text{Ar}$ and ΔAr) it appears the model overestimates cooling in the North Atlantic (model ΔAr is too negative at BATS), but may underestimate cooling in the Southern Ocean (model $\Delta\text{Kr}/\text{Ar}$ and ΔAr is not low enough in the

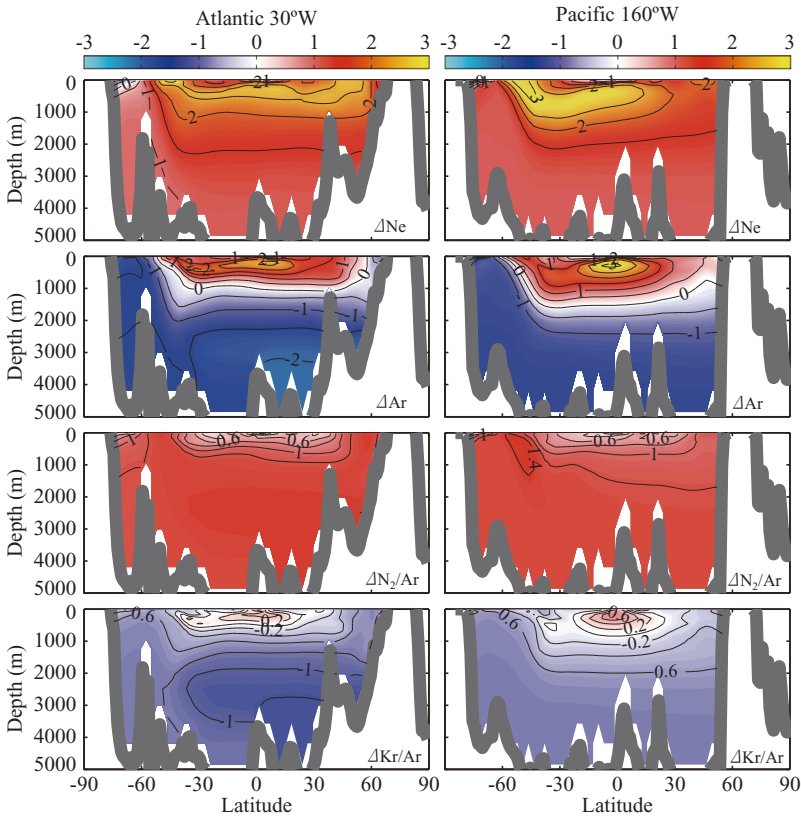


Figure 4 Interior distribution of saturation anomaly (percent) of ΔNe , ΔAr , $\Delta\text{Kr}/\text{Ar}$ and $\Delta\text{N}_2/\text{Ar}$. N-S sections are shown through the Atlantic (left) and Pacific (right).

Pacific). Also, given that higher winter wind speed may disproportionately contribute to the bubble signal that is subducted to the interior, our parameterization may overestimate high latitude bubble flux relative to wind speed.

Another intriguing possibility is that a measurable amount of N_2 could accumulate in older Pacific deep water due to denitrification, or that ice shelf melting in the Southern Ocean could elevate N_2 and Ne (Hohmann *et al.* 2002; Schlosser *et al.* 1990). These potential effects are small, but could explain why observed $\Delta\text{N}_2/\text{Ar}$ and ΔNe appear to slightly exceed model results in the Pacific, but are slightly lower in the Atlantic. Such processes are not included in our inert gas model, and if important, could lead to an overestimate of A_{inj} by up to about 10-20% (based on weighting Atlantic ΔNe and $\Delta\text{N}_2/\text{Ar}$ much higher than Pacific observations in the model inversion). The combined effect of these potential

sources of bias is that our estimate of A_{inj} should be considered an upper bound.

For ΔAr , an undersaturation filled most of the deep ocean due to cooling and low atmospheric pressure (Figure 4). In the thermocline, there was a supersaturation signal due to diapycnal mixing and the nonlinearity of solubility (Gehrie *et al.* 2006; Ito and Deutsch 2006). ΔNe behaved in a similar fashion to ΔAr , but ΔNe is less sensitive to cooling and mixing processes and more sensitive to bubble fluxes, which caused an overall more positive saturation state. For $\Delta\text{N}_2/\text{Ar}$, the bubble flux dominates which caused the saturation anomaly to be positive almost everywhere. The North Atlantic and Southern Ocean had the largest saturation anomaly in the model results due to the high wind speeds in these regions. In the Pacific, high values were seen originating in windy intermediate water formation regions while in the Atlantic a positive signal is subducted with NADW. The $\Delta\text{Kr}/\text{Ar}$ field was negative through the deep ocean due to a combination of bubbles and cooling, both of which make $\Delta\text{Kr}/\text{Ar}$ more negative. The thermocline mixing signal is also evident.

5. Discussion

5.1 Model performance

Bubble injection is constrained much better than bubble exchange because $\Delta\text{N}_2/\text{Ar}$ is influenced almost exclusively by the bubble injection process, and can be measured more precisely than ΔNe or ΔAr . Constraining bubble exchange is further complicated because both cooling/warming and atmospheric pressure variations can influence gas ratios in a similar proportion to bubble exchange. Errors in how the model simulates cooling, atmospheric pressure and mixing effects propagate more strongly into the determination of exchange bubble flux than for injection bubble flux. Improved modeling techniques that better characterize seasonality would limit uncertainty in estimating the cooling/circulation and atmospheric pressure components and improve our ability to constrain the exchanging bubble flux.

5.2 Comparing results

Because of the potential biases discussed earlier, our parameterization should be considered an upper limit of the relationship for average winds. Gas supersaturation depends on the balance of bubble flux in, and diffusive flux out of the surface ocean. Thus, studies using a different parameterization for k would require different bubble flux rates to achieve the same level of bubble induced super-saturation.

To adjust our values to be applicable to instantaneous winds, we follow the methodology of *Wanninkhof* (Wanninkhof 1992) and assume a Rayleigh

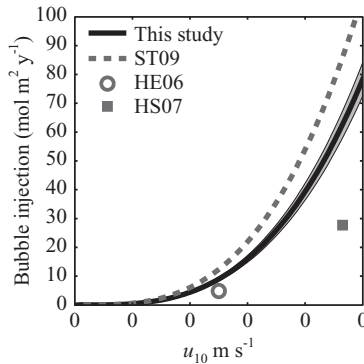


Figure 5 Solid black line shows injection flux and error (grey). Also shown are previous results from Stanley *et al.* (ST09), Hamme and Emerson (HE06) and Hamme and Severinghaus (HS07).

distributed wind speed. In our calculation, we have used averaged wind speeds to calculate both F_{bub} and k . Since F_{bub} scales with u^3 and k with u^2 we calculate that our parameters A_{inj} and A_{ex} should be adjusted to account for the non-linear relationship of both F_{bub} and k to wind speed:

$$A_{inst} = \frac{A_{ave}}{R}, \text{ where } R = \frac{\langle u^3 \rangle}{\langle u \rangle^3} \bigg| \frac{\langle u^2 \rangle}{\langle u \rangle^2} \approx 1.5 \quad (10)$$

where R is the flux enhancement factor (Wanninkhof *et al.* 2004), A is A_{inj} or A_{ex} , *ave* and *inst* refer to the A constant for instantaneous and average winds, respectively, and the brackets indicate averaging. To calculate bubble fluxes from instantaneous winds A_{inj} and A_{ex} should be reduced by one third.

Our inverse solution for injection flux ($A_{inj} = 2.51 \times 10^{-9}$) as a function of wind speed results in a flux from injecting bubbles somewhat less than the result of Stanley *et al.* (2009) who calculated a flux 40% higher than our result (Figure 5). The, Stanley *et al.* parameterization is based on a different wind product (6-hourly QuikSCAT) and a diffusive parameterization for k that was about 20% higher than Sweeney *et al.* (2007). After correcting for differences in k and multiplying by R , the comparable injection bubble flux for the Stanley *et al.* would be increased by an additional 15% and over 50% greater the result presented here.

Previous studies at HOT have found bubble injection flux to be somewhat lower. From upper ocean measurements of N_2 , Ar and O_2 , Hamme and Emerson (2006) inferred an injection flux of $6.8 \text{ mol air m}^{-2} \text{ yr}^{-1}$ for a mean wind speed of 7.1 m s^{-1} , compared to $13.1 \text{ mol air m}^{-2} \text{ yr}^{-1}$ (Stanley *et al.* 2009) and $9.5 \text{ mol air m}^{-2} \text{ yr}^{-1}$ for this study. At higher wind speeds, estimates diverge. Hamme and

Severinghaus (2007) reported an average injection flux of $27.7 \text{ mol air m}^{-2} \text{ yr}^{-1}$ for bubble injection during deep-water formation with mean wind-speed was 11.3 m s^{-1} . At an equivalent wind speed, our result was $62.7 \text{ mol air m}^{-2} \text{ yr}^{-1}$ and Stanley *et al.* (2009) estimate $85.9 \text{ mol air m}^{-2} \text{ yr}^{-1}$.

The differences in estimates of bubble injection is in part compensated for by the relative magnitude of bubble exchange in previous results. Hamme and Emerson (2006) found the lowest bubble injection, but highest proportion of bubble exchange flux, while Stanley *et al.* (2009) estimated that exchanging bubble flux accounted for only $\sim 15\%$ of total bubble flux for Ar (less than 5% for Ne and $\sim 25\%$ for Kr). Our result is intermediate between the two.

In general, our results add information for higher latitude regions with average wind speed up to about 12 m s^{-1} , where most previous work stems from seasonal variations in the subtropics, with wind-speeds closer to 7 m s^{-1} . Further observations at higher wind speeds ($15 + \text{ m s}^{-1}$) are needed to determine if injection flux continues to scale with wind speed cubed. With data currently available, our model does not constrain the flux of exchanging bubbles well, so it is difficult to compare the relative importance of each type of bubble. Our error range for V_{ex} does provide an upper limit estimate for the magnitude of bubble flux from exchanging bubbles. When calculated for argon using Equation 5, the exchanging flux could account for a maximum of about 50% of total bubble flux.

A predominance of injection bubbles relative to exchanging bubbles has significant consequences when scaling our results to compute bubble fluxes of CO_2 (and other more soluble gases). Injection bubble flux is negligibly small for CO_2 . Exchanging bubble flux scales with diffusivity, which is of the same magnitude for CO_2 and the inert gases. Calculated for $u_{10} = 10 \text{ m s}^{-1}$ and $T = 2^\circ\text{C}$ the CO_2 flux is $0.11 \pm 0.08 \text{ mol m}^{-2} \text{ yr}^{-1}$, which would be responsible for a 1.4 ± 1.0 matm steady-state supersaturation of $f\text{CO}_2$.

5.3 Future directions

The TMM method of simulating tracers proves to be an excellent laboratory to explore the effect of different parameterizations and processes on simulated gas distributions in the ocean interior. In this work, we constrain the magnitude of one bubble model using inert gas observations. Previous studies were based on subtropical mixed layer measurements, while this study extends bubble parameterization to include data from high latitudes and thus higher wind speed regimes.

The modeling method presented here can serve as the foundation for further efforts to incorporate noble gases into GCMs. As demonstrated, the TMM can lead to improved parameterizations of air-sea gas fluxes that could in the future be incorporated into full GCM simulations and applied to other gases. We anticipate

the next steps in improving the modeling methodology will be to use improved modeling methods to simulate the seasonal cycle (Khatiwala 2008) and use transport matrices created from other models. Resolving seasonality will allow the large number of upper-ocean observations to be better matched to model results as well as improve simulation of the conditions of deep water formation. Further observational constraints covering regions ventilated by a larger range of wind-speeds will make it possible to better distinguish the functional form of bubble fluxes as a function of wind-speed.

Many more yet unpublished inert gas measurements made by a number of research groups are not included in our model result. Adding additional observations as well as improving modeling methodology will enhance our understanding of not only air-sea bubble fluxes, but also the other physical processes that contribute to inert gas saturation state, such as the solubility pump and mixing within the thermocline. Accurately representing the distribution of inert gases on the global scale will provide the tools necessary to remove the 'abiotic' background component of the distribution of gases such as O₂ and CO₂ to better quantify the impact of biology.

Acknowledgments

Funding for much of the original sample collection and analysis was provided by NSF awards OCE-0647979 and OCE-0242139 to Steve Emerson and made possible through the technical assistance of Charles Stump, David Wilbur and Mark Haught at the University of Washington. David Nicholson would like to acknowledge valuable discussions with Taka Ito and Curtis Deutsch. Samar Khatiwala is supported by NSF Grants OCE 07-27229 and OCE 08-24635. This is LDEO contribution number 7433.

References

- Craig, H., and T. Hayward (1987), Oxygen Supersaturation in the Ocean: Biological Versus Physical Contributions, *Science*, 235(4785), 199-202, doi:10.1126/science.235.4785.199.
- Craig, H., and R. Weiss (1971), Dissolved gas saturation anomalies and excess helium in the ocean, *Earth and Planetary Science Letters*, 10(3), 289-296, doi:10.1016/0012-821X(71)90033-1.
- Dutay, J. -. *et al.* (2002), Evaluation of ocean model ventilation with CFC-11: comparison of 13 global ocean models, *Ocean Modelling*, 4(2), 89-120, doi:10.1016/S1463-5003(01)00013-0.
- Fuchs, G., W. Roether, and P. Schlosser (1987), Excess 3He in the ocean surface layer, *J. Geophys. Res. Oceans*, 92(C6), 6559-6568.
- Hamme, R. C., and S. R. Emerson (2002), Mechanisms controlling the global oceanic distribution of the inert gases argon, nitrogen and neon, *Geophys. Res. Lett.*, 29(23), 2120, doi:10.1029/2002GL015273.
- Hamme, R. C., and S. R. Emerson (2004), The solubility of neon, nitrogen and argon in

- distilled water and seawater, *Deep-Sea Res., Part I*, 51(11), 1517-1528, doi:10.1016/j.dsr.2004.06.009.
- Hamme, R. C., and S. R. Emerson (2006), Constraining bubble dynamics and mixing with dissolved gases: Implications for productivity measurements by oxygen mass balance, *J. Mar. Res.*, 64(1), 73-95, doi:10.1357/002224006776412322.
- Hamme, R. C., and J. P. Severinghaus (2007), Trace gas disequilibria during deep-water formation, *Deep-Sea Research Part I*, 54(6), 939-950, doi:10.1016/j.dsr.2007.03.008.
- Hamme, R. (2003), Applications of neon, nitrogen, argon and oxygen to physical, chemical and biological cycles in the ocean, Ph.D., University of Washington, Seattle, WA.
- Hohmann, R., P. Schlosser, S. Jacobs, A. Ludin, and R. Weppernig (2002), Excess helium and neon in the southeast Pacific: Tracers for glacial meltwater, *J. Geophys. Res. Oceans*, 107(C11), 3198, doi:10.1029/2000JC000378.
- Ito, T., and C. Deutsch (2006), Understanding the saturation state of argon in the thermocline: The role of air-sea gas exchange and diapycnal mixing, *Global Biogeochem. Cycles*, 20(3), GB3019, doi:10.1029/2005GB002655.
- Jenkins, W. J., D. J. Webb, L. Merlivat, and W. Roether (1988), The Use of Anthropogenic Tritium and Helium-3 to Study Subtropical Gyre Ventilation and Circulation [and Discussion], *Philosophical Transactions of the Royal Society of London. Series A, Mathematical and Physical Sciences (1934-1990)*, 325(1583), 43-61.
- Jiang, S., P. H. Stone, and P. Malanotte-Rizzoli (1999), An assessment of the Geophysical Fluid Dynamics Laboratory ocean model with coarse resolution: Annual-mean climatology, *J. Geophys. Res. Oceans*, 104 (C11), 25, 623-25, 645, doi: 10.1029/1999JC900095.
- Keeling, R. F. (1993), On the role of large bubbles in air-sea gas exchange and supersaturation in the ocean, *Journal of Marine Research*, 51(2), 237-271.
- Khatiwal, S. (2007), A computational framework for simulation of biogeochemical tracers in the ocean (DOI 10.1029/2007GB002923), *Global Biogeochem. Cycles*, 21(3).
- Khatiwal, S., M. Visbeck, and M. A. Cane (2005), Accelerated simulation of passive tracers in ocean circulation models, *Ocean Model.*, 9(1), 51-69, doi:10.1016/j.ocemod.2004.04.002.
- Khatiwal, S. (2008), Fast spin up of Ocean biogeochemical models using matrix-free Newton-Krylov, *Ocean Model.*, 23(3-4), 121-129, doi:10.1016/j.ocemod.2008.05.002.
- Kistler, R., E. Kalnay, W. Collins, S. Saha, G. White, J. Woollen, M. Chelliah, W. Ebisuzaki, M. Kanamitsu, and V. Kousky (2001), The NCEP/NCAR 50-year reanalysis, *Bull. Am. Meteorol. Soc.*, 82(2), 247-268.
- Marshall, J., A. Adcroft, C. Hill, L. Perelman, and C. Heisey (1997), A finite-volume, incompressible Navier Stokes model for studies of the ocean on parallel computers, *J. Geophys. Res.*, 102(C3), 5753-5766, doi:10.1029/96JC02775.
- Matsumoto, K. et al. (2004), Evaluation of ocean carbon cycle models with data-based metrics, *Geophys. Res. Lett.*, 31, 4 PP., doi:200410.1029/2003GL018970.
- Monahan, E. C., and T. Torgersen (1990), The enhancement of air-sea gas exchange by oceanic whitecapping, *Air-Water Mass Transfer*, 608-617.
- Nicholson, D., S. R. Emerson, N. Caillon, J. Jouzel, and R. C. Hamme (2010), Constraining ventilation during deep-water formation using deep-ocean measurements of the dissolved gas ratios $^{40}\text{Ar}/^{36}\text{Ar}$, N_2/Ar and Kr/Ar , *J. Geophys. Res. Oceans*, doi: 10.1029/2010JC006152.
- Schlosser, P., R. Bayer, A. Foldvik, T. Gammelsrød, G. Rohardt, and K. O. Münnich (1990),

- Oxygen 18 and helium as tracers of ice shelf water and water/ice Interaction in the Weddell Sea, *J. Geophys. Res.*, 95 (C3), PP. 3253-3263, doi: 199010.1029/JC095iC03p03253.
- Spitzer, W. S., and W. J. Jenkins (1989), Rates of vertical mixing, gas exchange and new production: Estimates from seasonal gas cycles in the upper ocean near Bermuda., *J. Mar. Res.*, 47(1), 169-196.
- Stanley, R. H. R., W. J. Jenkins, D. E. Lott, and S. C. Doney (2009), Noble gas constraints on air-sea gas exchange and bubble fluxes., *J. Geophys. Res. Oceans*, 114, C11020, doi: 10.1029/2009JC005396.
- Sweeney, C., E. Gloor, A. R. Jacobson, R. M. Key, G. McKinley, J. L. Sarmiento, and R. Wanninkhof (2007), Constraining global air-sea gas exchange for CO₂ with recent bomb ¹⁴C measurements, *Global Biogeochem. Cycles*, 21, 10 PP., doi: 200710.1029/2006GB002784.
- Trenberth, K. E., J. G. Olson, W. G. Large, and N. C. F. A. R. (US) (1989), *A global ocean wind stress climatology based on ECMWF analyses*, National Center for Atmospheric Research.
- Wanninkhof, R. (1992), Relationship between gas exchange and wind speed over the ocean, *J. Geophys. Res.*, 97(C5), 7373-7381, doi:10.1029/92JC00188.
- Wanninkhof, R., K. F. Sullivan, and Z. Top (2004), Air-sea gas transfer in the Southern Ocean, *J. Geophys. Res. Oceans*, 109, C08S19, doi:200410.1029/2003JC001767.
- Weiss, R. F., and T. K. Kyser (1978), Solubility of krypton in water and sea water, *J. Chem. Eng. Data*, 23(1), 69-72.
- Zwally, H., J. Comiso, C. Parkinson, W. Campbell, F. Carsey, and P. Gloerson (1983), *Antarctic sea ice, 1973-1976: satellite passive microwave observations*, NASA.